Journal of Materials Chemistry C

Ion Diffusion Coefficients in Poly(3-alkylthiophenes) for Energy Conversion and Biosensing: Role of Side-Chain Length and Microstructure

Journal:	*Journal of Materials Chemistry C*
Manuscript ID	TC-ART-08-2020-003690.R1
Article Type:	Paper
Date Submitted by the Author:	05-Sep-2020
Complete List of Authors:	Harris, Jonathan; University of Arizona Ratcliff, Erin; University of Arizona, Department of Materials Science and Engineering

ARTICLE

Ion Diffusion Coefficients in Poly(3-alkylthiophenes) for Energy Conversion and Biosensing: Role of Side-Chain Length and Microstructure

Received 00th January 20xx,
Accepted 00th January 20xx

DOI: 10.1039/x0xx00000x

Jonathan K. Harris[a] and Erin L. Ratcliff[a,b,c]*

Conductive polymers are promising materials as active elements for energy storage and conversion devices due to mixed ion-electron conduction. The ion diffusion coefficient is a relative measure of the efficacy of ion transport, allowing for comparison between materials and electrochemical conditions. In this work, diffusion coefficients of hexafluorophosphate (PF_6^-) counterions in poly(3-alkylthiophene) (P3AT) materials are measured as a function of both side-chain length and microstructure using electrochemical impedance spectroscopy (EIS). For semi-crystalline films, the diffusion coefficient is found to be anomalous and nearly independent of applied electrochemical potential. The anomalous behavior of diffusion indicates that spin casting yields compact films with an enthalpic barrier to ion transport, attributed to ionic trapping. Diffusion coefficient values ~4 x 10^{-11} cm^2/s were measured for all films, indicating interchain spacing, in the absence of strong intermolecular interactions with the electrolyte, is not a viable design strategy to control ion transport. For the prototypical system of poly(3-hexylthiophene), we observe almost no potential dependence in ion transport for regioregular and regiorandom films of comparable molecular weight, with both exhibiting anomalous diffusion. Alternatively, changing the microstructure of poly(3-hexylthiophene) to a mostly amorphous, ion-imprinted structure yields ~280x increase in the diffusion coefficient to ~2 x 10^{-8} cm^2/s at 0.8 V vs. Ag/Ag^+ with ordinary diffusion properties. Collectively, these results indicate new insight into ion transport in conductive polymers, where ionic trapping effects can be mitigated through electrodeposition protocols over post-synthesis processing (i.e. spin coating).

Introduction

Conductive polymers have received considerable attention as active elements in (photo)electrochemical devices for water splitting,[1–5] redox-flow batteries,[6,7] Lithium batteries,[8] electrochemical supercapacitors,[9–11] electrochromics,[12] and light-emitting electrochemical cells.[13–15] Inherent material advantages include low cost and facile changes in opto-electronic and redox properties through synthetic design. From a surface science perspective, conductive polymers eliminate complications in oxidation-reduction reactions due to dangling bonds that introduce mid-gap states in inorganic materials.

The growing interest in conductive polymers for (photo)electrochemical cells makes understanding and controlling charge transport across length scales extremely important. In electrochemical systems, conductive polymers exhibit a hybrid electronic-ionic conduction. Electrochemical doping introduces electronic charge carriers that are Coulombically supported by counterions diffusing/migrating into the film. Generally, the fraction of electronic charge on a polymer is a function of electrochemical potential and a combination of chemical-electronic-physical connections, including: redox potentials of the monomers,[16] nature of the charge, rearrangement of the bonds to support the charge,[17,18] size of incoming counterions,[17,19,20] and ability of the polymer to swell in a given solvent.[21]

There is a renewed interest in ion transport in conductive polymers, especially for new materials. Recent efforts have focused on modification of side chains, which can have a significant effect on the volumetric polymer-electrolyte interface. For organic electrochemical transistors, increasing the hydrophilicity of polymer side chains can increase polymer solvent uptake and ion transport in aqueous-based electrolytes; however too much solvent uptake can disrupt domain connectivity, decreasing charge mobility and performance.[17,22,23] Alternatively, polymer electrolytes can reduce the phase separation between polymer and electrolyte, which increases light emitting electrochemical device efficiency but at the cost of response time.[15,24] A common theme is noted: polymer relaxation and swelling increases the efficacy of ion penetration into the film but electrical charge mobility decreases due to the swelling of the solvated polymer chains.

[a] Department of Chemical Engineering, University of Arizona, 1133 E. James E Rogers Way, Tucson Arizona 85721, United States
[b] Department of Materials Science and Engineering, University of Arizona, 1235 E. James E Rogers Way, Tucson Arizona 85721, United States
[c] Department of Chemistry and Biochemistry, University of Arizona, 1306 E. University Way, Tucson, AZ 85721, United States
* ratcliff@email.arizona.edu

Electronic Supplementary Information (ESI) available: additional GIWAXS, cyclic voltammetry, electrochemical impedance, and ion diffusion coefficient data and discussion of ordinary versus anomalous diffusion and fitting. See DOI: 10.1039/x0xx00000x

To date, the effects of polymer microstructure on these competing design principles is not clear.[22,25] From polymer electrolyte literature, conflicting results on the most ideal structure for ion transport have been posited, and it depends on many different variables.[26] In some cases, crystalline regions are thought of as poor ion conductors,[27,28] but others report specifically designed crystalline microstructures with good ion transport.[29] Previous reports show a weak dependence of diffusion coefficient on polymer side chain length, but do not provide a structural rationale for this behaviour.[30] The trade-off between these properties can be characterized by the measurement of ion diffusion coefficients through films of varying microstructure across multiple length scales.

Herein, we investigate the class of semi-crystalline poly(3-alkylthiophenes) (P3ATs). For broad applicability to energy conversion systems and to avoid degradation and/or Faradaic contributions from water, we conduct all analysis in dry acetonitrile, a known suitable solvent for swelling in P3ATs over water (see supplemental information Figure S1).[31,32] In this work, the diffusion coefficient of hexafluorophosphate (PF_6^-) counterions in P3AT materials are measured as a function of both side-chain length and microstructure using electrochemical impedance spectroscopy (EIS). The advantage of EIS is the ability to resolve dynamic events in the frequency domain, allowing for separation of fast electronic processes from slower mass transport considerations. EIS of polymer electrodes at various oxidation potentials has been historically performed for many different polymers, including polyaniline[33] and polypyrrole.[34]

We first consider small incremental variations in the side chain length of the P3AT materials class. In poly(3-hexylthiophene) (P3HT), counterions have been proposed to sit in the (h00) plane of the crystallite.[31,35,36] However, changing the alkyl length in this system does little to alter the potential-dependent ion diffusion coefficient despite systematic increases in the (h00) plane, as measured by grazing incidence wide-angle x-ray scattering. This result suggests that despite the incremental increases in solution processability through an increase in the length of side chain, it is not a dominant design criteria for good ion transport. Thus, materials can be selected for redox properties and functionality (i.e. electrical conductivity) as a first approximation for inclusion in photoelectrochemical systems.

We then focus our attention on nanoscale effects, where we consider three model microstructures relevant for electrochemical devices: commercially available regioregular (RR) and regiorandom (RRa) P3HT, both of similar molecular weight, and an electrochemically deposited P3HT. The latter system was included as it can be simultaneously synthesized and deposited in the presence of counterions using a previously described potential-pulse protocol.[37] The systematic variance of microstructure of the same polymer provides insight into the impact of polymer processing on the hybrid ionic-electronic transport properties. Surprisingly, the regiorandom and regioregular films exhibit similar ion transport coefficients, with diffusion becoming independent of oxidation voltage after a critical voltage. As hypothesized, the electrochemically deposited P3HT has the highest diffusion coefficients, reaching a maximum of ~2 x 10^{-8} cm^2/s at 0.8 V vs Ag/Ag^+, which corresponds to a fully oxidized film. Our results suggest that including the counterion during the synthesis and/or deposition step, analogous to molecularly imprinted polymers, is strategic to control ion transport.

Materials and Methods

Film Fabrication

The following regioregular polymers and molecular weights were purchased from Rieke Metals: poly(3-butylthiophene) (P3BT) MW = 41 kg/mol, poly(3-hexylthiophene) MW = 58 kg/mol, poly(3-octylthiophene) (P3OT) MW = 54 kg/mol, poly(3-decylthiophene) (P3DT) MW = 62 kg/mol, and poly(3-dodecylthiophene) (P3DDT) MW = 39 kg/mol. Regiorandom P3HT MW = 47 kg/mol was also purchased from Rieke Metals. Films were fabricated via spin casting from 10mg/mL dichlorobenzene solutions at 1000 rpm and annealed at 120°C for 20 minutes in air before electrochemical testing. Electrochemically deposited films were made from an electrolyte comprised of 10 mM 3-hexylthiophene monomer (Sigma-Aldrich, ≥99%) in 0.1 M tetrabutylammonium hexafluorophospahte (TBAHFP, TCI America, Inc., 98%) in acetonitrile (Fisher Scientific, 98%), as outlined previously.[37] Briefly, ITO-coated glass slides (Colorado Concept Coatings LLC, 9-15 Ω sheet resistance) were etched with an aqueous hydroiodic acid (Sigma-Aldrich, 57 wt.%, 99.99%) before immersed for 12 hours in a 10 mM 3-thiophene acetic acid (Sigma-Aldrich, 98%) solution in acetonitrile to functionalize the surface with thiophene monomer. After immersion, these films were grown by chronoamperometry in the 3-hexylthiophene containing electrolyte, with an initial 0.5 seconds activation step at 1.4 V, then held at an oxidizing potential of 1.35 V for 20 seconds (vs. Ag/Ag^+ in 0.01 M $AgNO_3$ (BASi) and 0.1 M TBAHFP in acetonitrile). Film thicknesses were estimated with profilometry using a KLA-Tencor P15 (KLA Corporation), using 3 different films each and 3 sample points per film.

Electrochemical Characterization

Cyclic voltammograms were performed at a scan rate of 50 mV/sec in 0.1 M TBAHFP in acetonitrile, using a clean silver wire counter electrode and Ag/Ag^+ reference electrode in 0.01 M $AgNO_3$ and 0.1 M TBAHFP in acetonitrile on a CH Instruments 920D potentiostat (CH Instruments). Electrochemical impedance spectroscopy (EIS) was performed in the same electrochemical cell set-up after three cyclic voltammograms. A 10 mV amplitude sinusoidal input voltage was imposed on an offset voltage for different oxidation states of the polymer, with 5 minutes of constant DC bias applied prior to EIS to allow for cell equilibration. Equivalent circuit fitting was conducted in Zview software (Scribner Associates, Inc) for frequency range 68120 -2.15 Hz. Results were repeated for three different films of each chosen polymer. Full data for all polymers and repeated films can be found in the supplementary information, tabulated in a .xls file.

GIWAXS Measurements

Grazing-incidence wide-angle x-ray scattering (GIWAXS) measurements were carried out on beamline 11–3 at the Stanford Synchrotron Radiation Light Source (SSRL). The beam was kept at an energy of 13 keV and the incident angle of measurement was ~0.11 to 0.13°. Calibration of wavelength and sample-detector distance used a LaB_6 standard sample. Two-dimensional detector images were corrected from intensity versus pixel position to intensity versus q-spacing using giwaxstools and nika softwares in Igor.[38] Images were reduced to 1D plots via integration of cake segments and analyzed using the Multi-peak fit package in Igor.

Results and Discussion

Side chain length in P3ATs

Semicrystalline P3HT has served as the prototypical system for investigations into structure-property relationships in organic electronics. The polymer is comprised of nanoscale crystallites and amorphous domains interconnected through tie-chains, where the microstructure evidentially has significant impact on functionality. In electrochemical systems, this complex microstructure has been hypothesized to impact both the ionic and electronic transport properties. For example, prior studies on structure-property relationships of electrochemically doped, semicrystalline P3HT electrodes in ionic liquid[35] and acetonitrile[31] have demonstrated a voltage-dependent device performance, with emphasis on electronic and ionic charge transfer between aggregated and amorphous regions of the polymer as it is oxidized. Structurally, an increase in the alkyl plane (h00) with increased electrochemical doping (anodic potential) has been observed, with little change to the π-π stacking plane (0k0).[31,35,36] As such, we postulated that altering the side chain spacing could alter the ion transport properties.

Microstructure and electronic properties as a function of side-chain length

Grazing incidence wide-angle x-ray scattering was performed for films of 5 different chain lengths: -butyl (P3BT), -

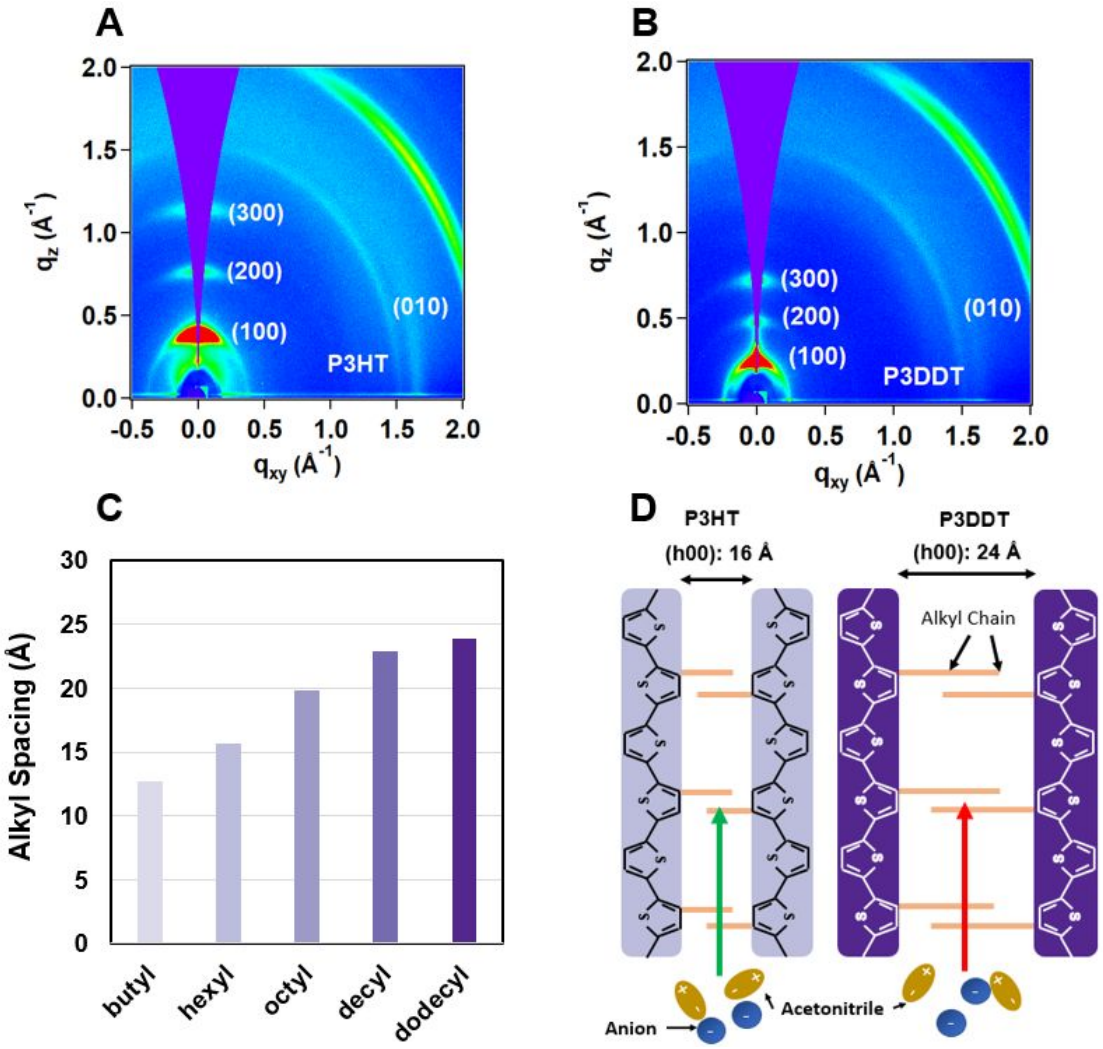

Figure 1: Two-dimensional grazing incidence wide-angle x-ray scattering (GIWAXS) detector images of (A) poly(3-hexylthiophene) (P3HT) and (B) poly(3-dodecylthiophene) (P3DDT). (C) Alkyl spacing of the five different chain lengths from -butyl to -dodecyl as measured from GIWAXS. (D) Schematic representation of alkyl spacing (h00) and pi-pi spacing (0k0), as a function of alkyl side chain length.

hexyl (P3HT), -octyl (P3OT), -decyl (P3DT), and -dodecyl (P3DDT) to first characterize the effect of poly(3-alkylthiophene) chain length on initial alkyl chain spacing differences. Figures 1A and 1B show the two-dimensional detector images for P3HT and P3DDT, respectively. Figure S2 in the supplemental information section provides the additional 2D detector images for the other polymers and Figure S3 shows the one-dimensional GIWAXS plots of cake slices in the q_z (out-of-plane) and q_{xy} (in-plane) directions. Estimated intermolecular spacings are provided in Table S1. In Figures 1A and 1B, the two crystallographic planes associated with the interdigitated alkyl chains (h00) and the π-π stacking (0k0) have been identified. It is qualitatively apparent from these 2D GIWAXS plots that there are differences in spacing between the hexyl and dodecyl side chains. All films exhibit an edge-on orientation relative to the substrate, with greater intensity of the (h00) diffraction peaks in the q_z over the (0k0) diffraction peak in the q_{xy} plane, as observed in the detector images Figures 1A and 1B, Figure S2, and the integrated intensity versus angle chi plots in Figure S4.

Figure 1C provides the determined alkyl plane (h00) spacings for the five polymer films and Figure 1D shows a schematic of the intermolecular distances in the alkyl plane. Corresponding pi-pi spacings for the (0k0) plane are given in the supplemental information section Figure S2 and Table S1. In Figure 1C, increasing the side chain length from four to twelve carbons corresponds to an 11 Å increase in the (h00) direction. These results are expected for the P3AT system, and the spacing values agree with previous experiment and simulation.[39] The measured pi-pi spacing (Figure S2) varied by approximately 0.2 Å between films, but did not exhibit an apparent linear correlation with side chain length.

To determine if the side chain length altered electronic properties, cyclic voltammetry was used to evaluate onset oxidation potentials. Figure 2 shows the cyclic voltammograms for P3HT and P3DDT for a direct comparison with Figure 1; all other cyclic voltammograms are provided in the supplementary info Figure S5. In Figure 2, we readily note the presence of two reversible oxidation waves for both polymeric systems, indicative of at least two unique electronic environments. These two environments have been recently summarized in the literature.[30,31,37,40–43] For P3HT, the peak near 0.2 V vs. $Ag/AgNO_3$ represents easier to oxidize aggregated domains of smaller band gap and larger conjugation length, while the peak near 0.6 V represents the amorphous regions with short conjugation length that is harder to oxidize.[43] Oxidation peak positions are noted with red dashed lines and show increases in oxidation potential for both amorphous and aggregate regions of the polymers as side chain increases.

To date, there have been a number of correlations in the role of microstructure associated with side-chain length on the electronic functionality of P3ATs. Intramolecularly, a more anodic potential (harder to oxidize) with increasing side chain length has been correlated to shorter conjugation lengths, which have less of an ability to delocalize charge over multiple polymer units.[35] Intermolecularly, longer side chains have been proposed to yield poorly ordered aggregates with lower interchain coupling,[44] which is further supported by a decrease

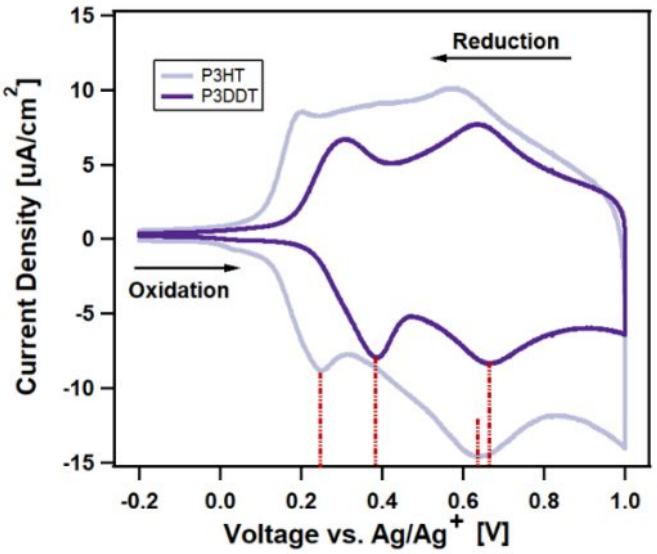

Figure 2: CV comparing P3HT to P3DDT. Films were run at 50 mV/s in acetonitrile with 0.1 M TBAHFP supporting electrolyte vs. 0.01 M Ag/Ag^+. Oxidation peak positions for aggregate and amorphous regions outlined to show the increase in oxidation potential for longer side chains.

in polymer melting temperature.[45] A secondary hypothesis then arises: the aggregate nature of the films, as defined by side-chain length, will affect the ion diffusion coefficient. Specifically, the electronic properties of the film aggregates could have some effect on ion diffusion coefficient, which can be measured through electrochemical impedance spectroscopy.

Electroanalytical Approaches for Determining Ion Diffusion Coefficients

Several electrochemical approaches have been used to measure ion diffusion coefficients in conductive polymers. The two most prevalent are chronoamperometry and electrochemical impedance spectroscopy. In the chronoamperometry approach, a change in the electrochemical potential (via a shift in applied bias) induces a transient current as the system undergoes transport processes to reach the new electrochemical potential. A common data analysis approach is to use the Cottrell equation to extract an ion diffusion coefficient from a chronoamperogram:

$$(1) \quad I = zFAC\sqrt{\frac{D}{\pi t}}$$

where z is the integer charge, F is Faraday's constant, A is the area of the electrode, and C is the concentration, traditionally formulated for redox-active analyte diffusing toward a metal electrode.[46] Interpretation requires the assumption that due to electroneutrality conditions, each injected positive charge (hole) on the polymer is counter-balanced by the incorporation of an anion. Thus, the apparent diffusion coefficient (D) is dependent upon the collective environment, as defined by the local structure, oxidation level, and ionic radii of the diffusion species:[47]

$$(2) \quad D = \frac{D_e D_i C_T}{D_e C_e + D_i C_i}$$

where D_e and D_i are the diffusion coefficients of electrons/holes and ions respectively, C_e and C_i are the associated

concentrations, and C_T is the total concentration. However, carrier densities can be on the order of 10^{16} to 10^{20} cm^{-3} while ion insertion is linearly dependent on potential.[31] A secondary challenge is the Cottrell equation given in (1) above is a 1D planar solution and ignores anomalous diffusion considerations – such as nucleation sites for charge transfer, porous media effects, and the known microstructure-controlled charge transport mechanism of poly(3-alkylthiophenes). Specifically, for semicrystalline P3HT, microstructure is changing during oxidation, where the accumulation of electrical charge on aggregates can facilitate charge transfer to the disordered amorphous regions that precedes conformational relaxation of the crystallites to accommodate counterions. [31]

Alternative to a chronoamperometry approach, electrochemical impedance spectroscopy (EIS) is conducted as a small perturbation to an existing steady-state condition. In EIS, a small sinusoidal AC waveform (typically 5-10 mV) is applied on top of a DC bias after the film has reached an established electrochemical potential. The advantage of EIS is the ability to resolve dynamic events in the frequency domain, allowing for separation of fast electronic processes from slower mass transport considerations, thus separating out the diffusion components in Equation 2. While EIS has gained some criticism for requiring a physical model biased by the experimentalist,[48] it requires and implicates deeper understandings about the electrochemical system at hand through equivalent circuit modelling of relevant characteristics for polymer devices.

EIS of electroactive polymers has been investigated in previous literature, namely by Bisquert and De Levi.[30,49–51] Of particular note, Bisquert and Compte[50] proposed an anomalous diffusion model of ions, where the flux condition is described as

$$(3)\quad \frac{d^{\gamma}n}{dt^{\gamma}} = -\frac{dJ}{dx}$$

where n is the number of ions, t is time, and J is flux along some relevant length scale x. In most typical electrochemical applications, ordinary diffusion is assumed (γ = 1), stating the number of ions entering/leaving a given system is directly proportional to the flux distribution of the given ion (mass is conserved). If 0 < γ < 1, this suggests that the amount of ion flux into the system is not conserved, physically understood for these systems that there is a distribution of energy sites upon which diffusing ions can be trapped and rendered immobile. This departure from ordinary diffusion is termed "anomalous", developed to describe transport through structurally complex systems. A more detailed explanation is provided in the SI section.

An anomalous diffusion model draws parallels to the established electronic charge transport models in organic semiconductors. Briefly, the distribution of the trap states is related to the paracrystallinity of the polymer, with more disordered polymers having higher amounts of trap states with deeper energy wells.[52] Therefore, transport in the amorphous regions of P3HT can be described by a multiple trapping and release (MTR) mechanism,[53,54] that describes carriers as hopping from state to state, some of which can trap charge carriers.

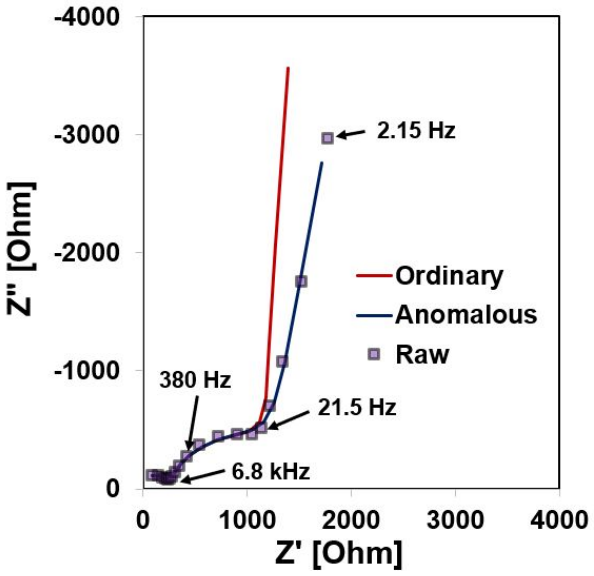

Figure 3: Example of an anomalous diffusion fit vs. ordinary diffusion fit for the raw Nyquist EIS data of a P3HT film at 0.3 V vs. 0.01M Ag/Ag+. Electrochemical cell is acetonitrile with 0.1 M TBAHFP supporting electrolyte.

Figure 3 shows the raw data for a Nyquist plot of a spin cast P3HT electrode at 0.3 V with both the ordinary and anomalous diffusion fits. It has been shown previously that a simple Randles' circuit can be used to examine an electroactive polymer,[55] and to account for charge transfer across varying interfaces, an extra parallel resistor and constant phase element (R-CPE) in series is required,[56] as shown in Figure S6. From Figure 3, it is readily apparent that ordinary diffusion has poor agreement with the lower frequency, mass diffusion regime. Full EIS spectra with fits are shown in Figures S7-S13 and full tabulated data can also be found in the supplementary information as a .xls file.

Estimation of the diffusion coefficient assumes a reflecting boundary (ions do not diffuse into the metal contact). Fick's Law can be solved with the fractional continuity equation to yield the impedance of non-ordinary diffusion (Equation 4)

$$(4)\quad Z = R_o\left(\frac{i\omega}{\omega_d}\right)^{-\beta}\coth\left[\left(\frac{i\omega}{\omega_d}\right)^{-\beta}\right]$$

where R_0 describes a diffusion resistance related to the geometry of the film, ω is the input frequency, ω_d is the characteristic frequency, and β (0 < β < 1) is the anomalous diffusion parameter. β is equal to 0.5 for ordinary Warburg diffusion. The estimation of ω_d is used to extract the diffusion coefficient D_o with the thickness of the film L by equation 5:

$$(5)\quad \omega_d = \left(\frac{D}{L^2}\right)^{\frac{1}{\beta}}$$

Figure 4 provides voltage-dependent diffusion coefficients for the five different side chain films, where all exhibit highly anomalous behaviors (β ≈ 1), indicating ionic trapping effects. We readily note in Figure 4 that we exclude values estimated below 0.2 V (red box), where the films are still considerably compact and we cannot justifiably separate diffusion in electrolyte versus polymer. Previous potential-dependent

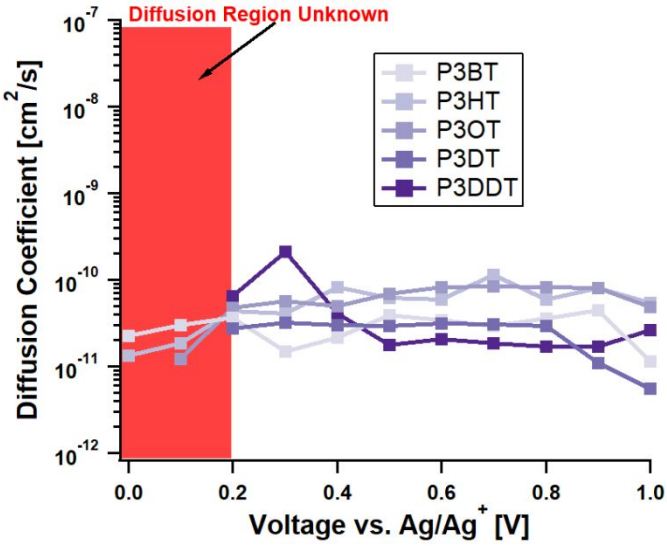

Figure 4: Diffusion coefficients of different P3ATs at different voltages vs. 0.01 M Ag/Ag^+, showing that diffusion is nearly independent of side chain length and voltage (past a certain voltage). These films were chosen as best representations for the average of each film (Figure S15).

GIWAXS for P3HT shows no effect on crystalline regions up to 0.2 V, which supports the ambiguity of these values.[31] Exclusion of this regime was determined due to the ion diffusion coefficient in the solvent measured at ~10^{-7} cm^2/s as well as the sample to sample variability shown in Figure S16). In Figure 4, it is evident that the diffusion coefficients are nearly independent of voltage. Plots of the anomalous diffusion parameter β are shown in Figure S17, with all being generally anomalous ($\beta \neq 0.5$). This suggests heterogeneous effects within the films (i.e. microstructure) cannot be overcome with voltage, again consistent with the proposed ion trapping mechanism of anomalous diffusion. The results here are shown to vary over half an order of magnitude about $(4 \pm 2) \times 10^{-11}$ $cm^2\ s^{-1}$. Despite the changes in electronic properties and microstructure, there is a weak dependence of diffusion coefficient on polymer chain length, consistent with other polymer-electrolyte systems.[30] Likewise, we observed no statistical trend in the differences in molecular weight when considering all films (Figure S15). This suggests that to design a polymer electrochemical system that provides significant gains in mass transport, length of alkyl side chains provide a lesser role in the absence of strong intermolecular interactions between side-chain and solvent. However, the effect of side chain length on ion transport may be more impactful in polar solvents and/or in the presence of heteroatoms, such as the effect of glycolated and/or alcohol groups when water is used as the solvent.[57]

Microstructure Effects in P3HT

As side chain was shown to have little effect and diffusion was found to be anomalous in the regioregular polymers, we then consider the role of microstructure on ionic transport. Of particular note, electrochemical strain microscopy

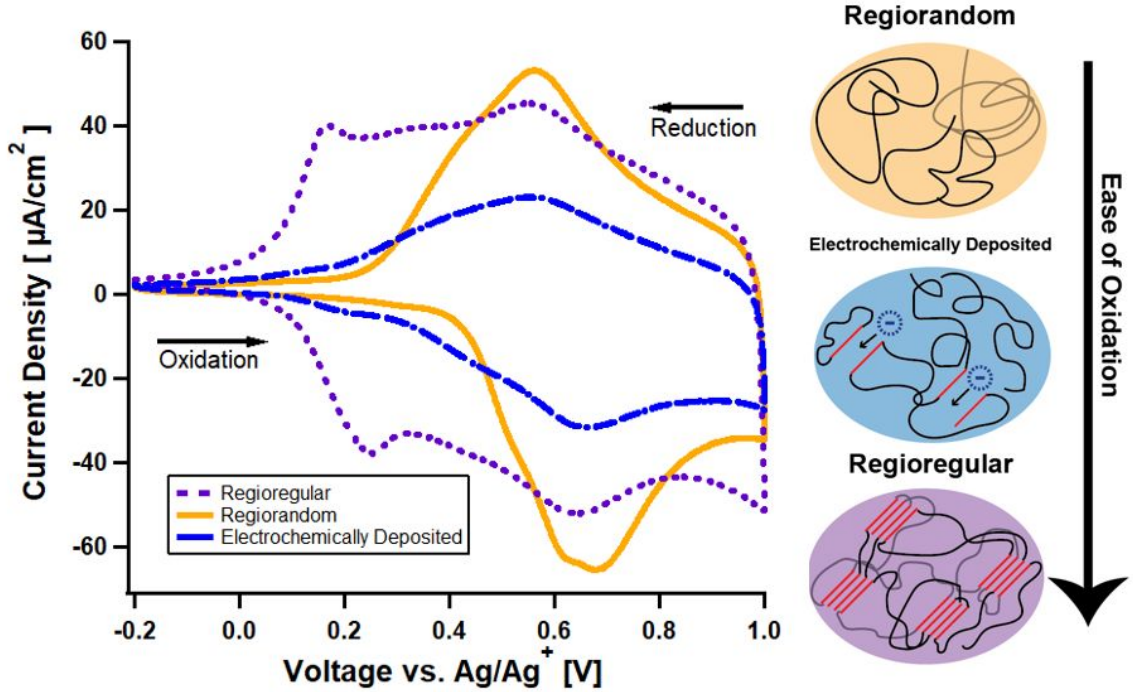

Figure 5: Cyclic voltammograms of three distinct microstructures of P3HT, with microstructure representations on the right. Scan rate of 50 mV/s, in acetonitrile with 0.1 M TBAHFP supporting electrolyte. Reference electrode is Ag/Ag^+ with 0.01 M $AgNO_3$.

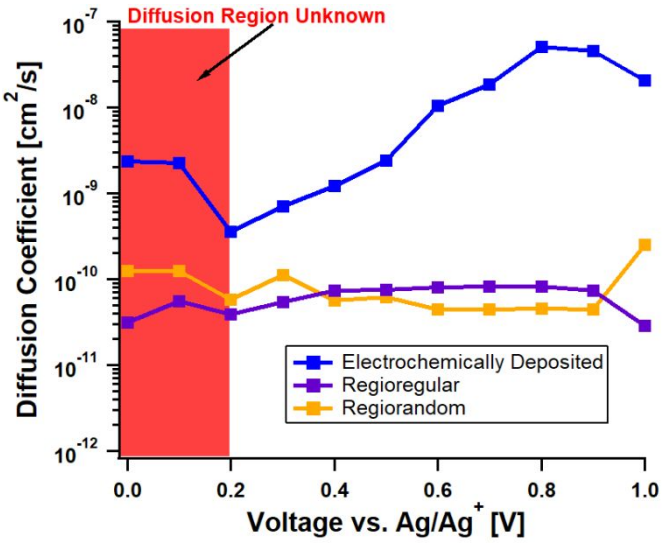

Figure 6: Diffusion coefficients for single films representing different microstructures of P3HT vs 0.01 M Ag/Ag^+. These films were chosen as best representations for the average of each film (Figure S16). Red box indicates voltage independent data when diffusion is not occurring through polymer film.

measurements of P3HT in water show that upon oxidation, ions travel in to regions with low elastic modulus, corresponding to the amorphous regions of the film,[19] which would suggest that amorphous materials may have higher diffusion coefficients. Additionally, there has been recent reports of reversible phase-transformations in select systems focused on use in water.[58] Thus we next turn our consideration to microstructure effects in our system, focusing on comparing regioregular, regiorandom, and electrodeposited P3HT. The latter was included as electrochemically deposited films are grown in such a way (as detailed in the Methods section) that during the electro-synthetic process, the film remains relaxed, electrochemically oxidized, and ions are retained.[37,41,56] It is postulated that the amorphous regions could behave similarly to a molecularly imprinted polymer and will exhibit increased ion transport over the spin cast films.

Redox properties were investigated by cyclic voltammetry (Figure 5) and have been previously described.[31,37,40,41] Regioregular P3HT has the lowest onset potential for oxidation, from the presence of well-ordered aggregates evident in UV-Vis spectra.[31] Electrochemically deposited P3HT has the next lowest onset potential for oxidation, and is shown through GIWAXS to be mostly amorphous.[40] Although regiorandom is also amorphous, the electrochemically deposited films have the presence of PF_6^- ion pathways included during film fabrication,[37] which could contribute to having regions slightly easier to oxidize than regiorandom films spun in air.

The potential-dependent diffusion coefficients for the three microstructures are shown in Figure 6 for single films, estimated using the anomalous diffusion model; Figure S16 provides diffusion coefficients for three films and the average diffusion coefficient with respect to potential for each microstructure. Interestingly, the regiorandom and regioregular P3HT exhibit statistically similar ion diffusion properties, despite the semicrystallinity of regioregular P3HT. This suggests that the limiting factor for apparent diffusion is associated with the amorphous domains of the polymer, although these may not be co-equal in regioregular and regiorandom films. In other words, spin casting results in a considerably close-packed film (non-porous) and ion diffusion is dominated by the structural relaxation of the film in the amorphous domains, as ions attempt to create volumetric void. Plots of β, which signifies departure from Warburg diffusion (β = 0.5), are included in the Si Figure S17. These plots show that highly anomalous diffusion occurs for the spin coated films of regioregular P3HT, and that electrochemically deposited films approach normal unimpeded diffusion. Considering Bisquert's description of ion movement in polymer electrodes,[59] this suggests that the electrochemically deposited films have less traps.

Also evident in Figure 6 is that the electrochemically deposited film has significantly larger ion diffusion coefficients than the other two microstructures. Unlike conventional cyclic voltammetry used for electrodeposition, the potential pulse profile that was used retains the film under constant state of high oxidation and is mass transfer limited for thiophene monomer deposition. This results in a three-dimensional nucleation and growth of the polymer film, where the PF_6^- anions are continuously incorporated into the film through ion transport channels.[37,60] We postulate that these ion channels, formed during the combined synthesis and deposition, are what are giving rise to the large ion diffusion coefficients. Diffusion coefficients measured without any polymer are around 2×10^{-7} cm^2/s, and these electrodeposited films approach those values. Here we see the expected potential-dependent behavior of ion diffusion consistent with Eyring rate theory extrapolated to electrochemical systems, whereby an application of a voltage results in a lowering of activation energy (here assumed to be enthalpic). This can be interpreted as the change in the electrochemical potential, associated with a change in the voltage, modifies the film microstructure in such a way to allow for more efficacious ion transport.

Diffusion coefficients at a potential of 0.8 V for three films of each various microstructure are shown in Table 1. The results from other studies of EIS of conducting polymer electrodes is included in the table for reference, and interestingly show similar diffusion coefficients for electrochemically deposited polypyrrole[23] and spin-coated films in one study. This may be a result of differences in low-frequency analysis; Panero et al.[61] define diffusion during a "limiting capacitance" circuit element as the film is fully oxidized, and do not consider the anomalous diffusion effects outlined later by Bisquert.[49] There are also differences by a few orders of magnitude in the Tanguy et al.[34] study, most likely due to differences in film fabrication, as their films were drop cast from a chloroform solution. The ESCR model has also been utilized by Otero et al. to analyse electrochemically deposited polypyrrole and found values ~10^{-9} cm^2/s which is similar to the electrochemically deposited P3HT in this work.[62] The disparity of these results necessitates a complementary technique to confirm the diffusion mechanism in specific film microstructures and how well it can be probed by various electrochemical techniques.

Conclusions

Table 1: Diffusion coefficients in electrochemical environments for various polymers in this work and literature for comparison.

Polymer, Anion	Diffusion Coefficient [cm^2/s]	Ref.
RR-P3HT, PF_6^-	$(7 \pm 1) \times 10^{-11}$	This Work
RRa-P3HT, PF_6^-	$(5 \pm 0.3) \times 10^{-11}$	This Work
Echem Dep P3HT, PF_6^-	$(2.2 \pm 2) \times 10^{-8}$	This Work
Echem Dep Polypyrrole, ClO_4^-	2×10^{-11}	Panero et al.[54]
P3HT, ClO_4^-	5×10^{-14}	Tanguy et al.[26]
P3OT, ClO_4^-	10^{-13}	Tanguy et al.[26]

Conductive polymers, as mixed-ion-electron conductors, exhibit conflicting design guidelines – the criteria that promotes good electron transport usually comes at the sacrifice of ion diffusion. This work further shows, with diffusion coefficients found through EIS and the anomalous transport model, that polymer aggregates and electronic environment play a smaller part on ion transport for P3ATs in acetonitrile. Varying the length of side chain in the P3AT system provide only very modest gains in transport, found to vary within half an order of magnitude for multiple films of each side chain length. We posit that for spin cast films, the end film is highly compact and ion transport is restricted due to an enthalpic barrier that cannot be overcome with electrochemical potential and doping. Specifically, we conclude there is a resistance to electrochemically stimulated conformational changes along the polymeric chains that limits the generation of free volume needed for rapid ion transport, even with electrochemical conditioning. This effect seems to be independent of microstructure (semi-crystalline versus amorphous) and side chain length. Thus we conclude that the spin cast polymers remain relatively compact, even when fully oxidized, which could be strategic for electronic carrier transport. Alternatively, the increase in nearly two orders of magnitude for the electrodeposited film indicates a prudent strategy for increased ion transport is to create a more porous material. From our results, we posit that the amorphous domains are capable of more rapid ion transport if longer-range ion channels can be developed. This is a current focus of future work, along with investigations of how other processing and synthetic strategies can be used to control charge transport in conductive polymer electrochemical devices.

Conflicts of interest

There are no conflicts to declare.

Acknowledgements

This material is based upon work supported by the U.S. Department of Energy, Office of Science, Office of Basic Energy Sciences under Award Number DE-SC0020208. Use of the Stanford Synchrotron Radiation Lightsource, SLAC National Accelerator Laboratory is supported by the U.S. Department of Energy, Office of Science, Office of Basic Energy Sciences under Contract No. DE-AC02-76SF00515. A portion of this work was performed in the Nanofabrication Center at the University of Arizona.

Notes and references

1 J. Kosco, M. Bidwell, H. Cha, T. Martin, C. T. Howells, M. Sachs, D. H. Anjum, S. Gonzalez Lopez, L. Zou, A. Wadsworth, W. Zhang, L. Zhang, J. Tellam, R. Sougrat, F. Laquai, D. M. DeLongchamp, J. R. Durrant and I. McCulloch, *Nat. Mater.*, , DOI:10.1038/s41563-019-0591-1.

2 F. Fumagalli, S. Bellani, M. Schreier, S. Leonardi, H. C. Rojas, A. Ghadirzadeh, G. Tullii, A. Savoini, G. Marra, L. Meda, M. Grätzel, G. Lanzani, M. T. Mayer, M. R. Antognazza and F. Di Fonzo, *J. Mater. Chem. A*, 2016, **4**, 2178–2187.

3 E. Lanzarini, M. R. Antognazza, M. Biso, A. Ansaldo, L. Laudato, P. Bruno, P. Metrangolo, G. Resnati, D. Ricci and G. Lanzani, *J. Phys. Chem. C*, 2012, **116**, 10944–10949.

4 R. S. Sprick, B. Bonillo, M. Sachs, R. Clowes, J. R. Durrant, D. J. Adams and A. I. Cooper, *Chem. Commun.*, 2016, **52**, 10008–10011.

5 G. Zhang, Z.-A. Lan and X. Wang, *Angew. Chem. Int. Ed.*, 2016, **55**, 15712–15727.

6 T. Janoschka, N. Martin, U. Martin, C. Friebe, S. Morgenstern and H. Hiller, *Nature*, 2015, **527**, 78+.

7 J. Chai, A. Lashgari, X. Wang, C. K. Williams and J. "Jimmy" Jiang, *J. Mater. Chem. A*, 2020, 10.1039.D0TA02303E.

8 Y. Fu and A. Manthiram, *Chem. Mater.*, 2012, **24**, 3081–3087.

9 J. Edberg, O. Inganäs, I. Engquist and M. Berggren, *J. Mater. Chem. A*, 2018, **6**, 145–152.

10 S. P. Arnold, J. K. Harris, B. Neelamraju, M. Rudolph and E. L. Ratcliff, *Synthetic Metals*, 2019, **253**, 26–33.

11 J. Wang, Y. Xu, X. Chen and X. Du, *Journal of Power Sources*, 2007, **163**, 1120–1125.

12 R. J. Mortimer, A. L. Dyer and J. R. Reynolds, *Displays*, 2006, **27**, 2–18.

13 J. Mindemark and L. Edman, *J. Mater. Chem. C*, 2016, **4**, 420–432.

14 Z. Zhang, K. Guo, Y. Li, X. Li, G. Guan, H. Li, Y. Luo, F. Zhao, Q. Zhang, B. Wei, Q. Pei and H. Peng, *Nature Photon*, 2015, **9**, 233–238.

15 Q. Pei, G. Yu, C. Zhang, Y. Yang and A. J. Heeger, *Science*, 1995, **269**, 1086–1088.

16 J. A. Irvin, I. Schwendeman, Y. Lee, K. A. Abboud and J. R. Reynolds, *Journal of Polymer Science Part A: Polymer Chemistry*, 2001, **39**, 2164–2178.
17 C. Cendra, A. Giovannitti, A. Savva, V. Venkatraman, I. McCulloch, A. Salleo, S. Inal and J. Rivnay, *Adv. Funct. Mater.*, 2019, **29**, 1807034.
18 M. Nowak, S. D. D. V. Rughooputh, S. Hotta and A. J. Heeger, *Macromolecules*, 1987, **20**, 965–968.
19 R. Giridharagopal, L. Q. Flagg, J. S. Harrison, M. E. Ziffer, J. Onorato, C. K. Luscombe and D. S. Ginger, *Nature Materials*, 2017, **16**, 737–742.
20 L. Q. Flagg, R. Giridharagopal, J. Guo and D. S. Ginger, *Chemistry of Materials*, 2018, **30**, 5380–5389.
21 A. Savva, C. Cendra, A. Giugni, B. Torre, J. Surgailis, D. Ohayon, A. Giovannitti, I. McCulloch, E. Di Fabrizio, A. Salleo, J. Rivnay and S. Inal, *Chemistry of Materials*, 2019, **31**, 927–937.
22 L. Q. Flagg, C. G. Bischak, J. W. Onorato, R. B. Rashid, C. K. Luscombe and D. S. Ginger, *J. Am. Chem. Soc.*, 2019, **141**, 4345–4354.
23 A. Giovannitti, D.-T. Sbircea, S. Inal, C. B. Nielsen, E. Bandiello, D. A. Hanifi, M. Sessolo, G. G. Malliaras, I. McCulloch and J. Rivnay, *PNAS*, 2016, 201608780.
24 Y. Yang and Q. Pei, *Journal of Applied Physics*, 1997, **81**, 3294–3298.
25 S.-M. Kim, C.-H. Kim, Y. Kim, N. Kim, W.-J. Lee, E.-H. Lee, D. Kim, S. Park, K. Lee, J. Rivnay and M.-H. Yoon, *Nat Commun*, 2018, **9**, 3858.
26 J. Mindemark, M. J. Lacey, T. Bowden and D. Brandell, *Progress in Polymer Science*, 2018, **81**, 114–143.
27 C. C. Lee and P. V. Wright, *Polymer*, 1982, **23**, 681–689.
28 A. Killis, J.-F. LeNest, H. Cheradame and A. Gandini, *Makromol. Chem.*, 1982, **183**, 2835–2845.
29 Z. Gadjourova, Y. G. Andreev, D. P. Tunstall and P. G. Bruce, *Nature*, 2001, **412**, 520–523.
30 J. Tanguy, A. Proń, M. Zagórska and I. Kulszewicz-Bajer, *Synthetic Metals*, 1991, **45**, 81–105.
31 J. K. Harris, B. Neelamraju and E. L. Ratcliff, *Chem. Mater.*, 2019, **31**, 6870–6879.
32 J. Roncali, L. H. Shi, R. Garreau, F. Garnier and M. Lemaire, *Synthetic Metals*, 1990, **36**, 267–273.
33 I. Rubinstein and E. Sabatani, *Journal of Electrochemical Society*, 1987, **134**, 3078–3083.
34 J. Tanguy, *J. Electrochem. Soc.*, 1987, **134**, 795.
35 J. O. Guardado and A. Salleo, *Advanced Functional Materials*, 2017, **27**, 1701791.
36 E. M. Thomas, M. A. Brady, H. Nakayama, B. C. Popere, R. A. Segalman and M. L. Chabinyc, *Advanced Functional Materials*, 2018, **28**, 1803687.
37 E. L. Ratcliff, J. L. Jenkins, K. Nebesny and N. R. Armstrong, *Chemistry of Materials*, 2008, **20**, 5796–5806.
38 S. D. Oosterhout, V. Savikhin, J. Zhang, Y. Zhang, M. A. Burgers, S. R. Marder, G. C. Bazan and M. F. Toney, *Chem. Mater.*, 2017, **29**, 3062–3069.
39 J. Corish, D. A. Morton-Blake, F. Bénière and M. Lantoine, *J. Chem. Soc., Faraday Trans.*, 1996, **92**, 671–677.
40 B. Neelamraju, M. Rudolph and E. L. Ratcliff, *J. Phys. Chem. C*, , DOI:10.1021/acs.jpcc.8b06861.
41 J. L. Jenkins, P. A. Lee, K. W. Nebesny and E. L. Ratcliff, *Journal of Materials Chemistry A*, 2014, **2**, 19221–19231.
42 J. Roncali, R. Garreau, A. Yassar, P. Marque, F. Garnier and M. Lemaire, *J. Phys. Chem.*, 1987, **91**, 6706–6714.
43 M. Skompska and A. Szkurłat, *Electrochimica Acta*, 2001, **46**, 4007–4015.
44 M. Al-Ibrahim, H.-K. Roth, M. Schroedner, A. Konkin, U. Zhokhavets, G. Gobsch, P. Scharff and S. Sensfuss, *Organic Electronics*, 2005, **6**, 65–77.
45 A. J. Heeger, P. Smith, M. F. Rubner and T. A. Skotheim, in *Conjugated Polymers*, Kluwer Academic Publishers, 1st edn., 1991, pp. 141–210.
46 A. J. Bard and L. R. Faulkner, *Electrochemical Methods: Fundamentals and Applications*, Wiley, New York, 2nd edn., 2001.
47 R. P. Buck, *J. Electroanal. Chem.*, 1987, **219**, 23–48.
48 I. J. Suárez, T. F. Otero and M. Márquez, *The Journal of Physical Chemistry B*, 2005, **109**, 1723–1729.
49 J. Bisquert, G. Garcia-Belmonte, F. Fabregat-Santiago and A. Compte, *Electrochemistry Communications*, 1999, **1**, 429–435.
50 J. Bisquert and A. Compte, *Journal of Electroanalytical Chemistry*, 2001, **499**, 112–120.
51 M. A. Vorotyntsev, L. I. Daikhin and M. D. Levi, *Journal of Electroanalytical Chemistry*, 1994, **364**, 37–49.
52 J. Rivnay, R. Noriega, J. E. Northrup, R. J. Kline, M. F. Toney and A. Salleo, *Phys. Rev. B*, 2011, **83**, 121306.
53 D. P. McMahon, D. L. Cheung, L. Goris, J. Dacuña, A. Salleo and A. Troisi, *J. Phys. Chem. C*, 2011, **115**, 19386–19393.
54 A. Salleo, T. W. Chen, A. R. Völkel, Y. Wu, P. Liu, B. S. Ong and R. A. Street, *Phys. Rev. B*, 2004, **70**, 115311.
55 R. Hass, J. García-Cañadas and G. Garcia-Belmonte,

Journal of Electroanalytical Chemistry, 2005, **577**, 99–105.

56 M. Rudolph and E. L. Ratcliff, *Nat Commun*, 2017, **8**, 1048.

57 M. Moser, L. R. Savagian, A. Savva, M. Matta, J. F. Ponder, T. C. Hidalgo, D. Ohayon, R. Hallani, M. Reisjalali, A. Troisi, A. Wadsworth, J. R. Reynolds, S. Inal and I. McCulloch, *Chem. Mater.*, 2020, **32**, 6618–6628.

58 C. G. Bischak, L. Q. Flagg, K. Yan, T. Rehman, D. W. Davies, R. J. Quezada, J. W. Onorato, C. K. Luscombe, Y. Diao, C.-Z. Li and D. S. Ginger, *J. Am. Chem. Soc.*, 2020, **142**, 7434–7442.

59 J. Bisquert, G. Garcia-Belmonte and Á. Pitarch, *ChemPhysChem*, 2003, **4**, 287–292.

60 E. L. Ratcliff, P. A. Lee and N. R. Armstrong, *Journal of Materials Chemistry*, 2010, **20**, 2672.

61 S. Panero, *J. Electrochem. Soc.*, 1989, **136**, 3729.

62 T. F. Otero, M. Márquez and I. J. Suárez, *J. Phys. Chem. B*, 2004, **108**, 15429–15433.

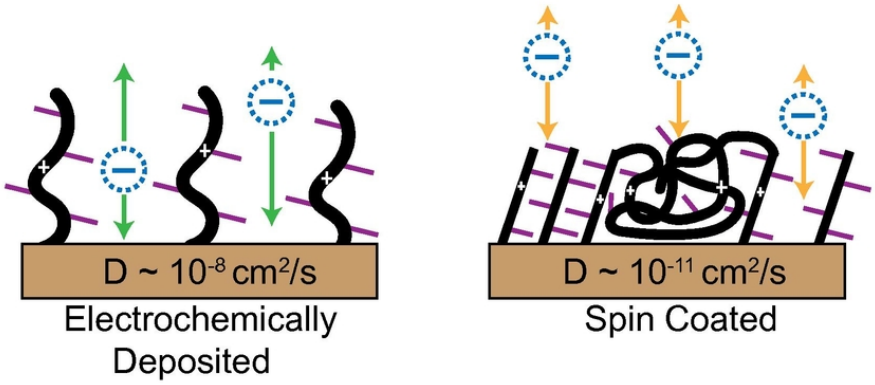

79x39mm (300 x 300 DPI)